Journal of Thermal Engineering
https://jten.yildiz.edu.tr/
https://doi.org/10.47481/jten.0087

RESEARCH ARTICLE

Flow dynamics behavior and thermal performance evaluation of double pipe counter flow heat exchanger with twisted tape inserts in the presence of hybrid nanofluids

Pidaparthy Maheshbabu[1,2], Ramkumar Ramkrishnan[3], Goda Sreenivasulu Reddy[4], Prakash H. Jadhav[5,*]

[1]Research Scholar, Department of Mechanical Engineering, Faculty of Engineering and Technology, Annamalai University, Annamalai Nagar, Tamil Nadu 608002, India
[2]Department of Mechanical Engineering, CMR College of Engineering & Technology, Hyderabad, Telangana 501401, India
[3]Department of Mechanical Engineering, Annamalai University, Annamalai Nagar, Tamil Nadu 608002, India
[4]Department of Mechanical Engineering, Mahatma Gandhi Institute of Technology, Hyderabad, Telangana 500075, India
[5]Faculty of Science and Technology, School of Mechanical and Manufacturing Sciences, JSPM University, Wagholi, Pune, Maharashtra 412207, India

Abstract

The performance of counter flow heat exchanger is analyzed with and without the insertion of sector cut twisted tape (TT) inserts in the presence of ZnO/MWCNT hybrid nanofluids (HNFs). The sector cut twisted tape inserts is positioned at the exit of tube heat exchanger (HEx). For the analysis, three different concentrations of hybrid nanofluids (0.01%, 0.03% and 0.05%) and three different sector cut twisted tape inserts (5 mm, 7 mm, and 9 mm) are employed. For numerical investigations, a standard two equations k-ε model is employed. The novelty of the study is to assess the influence of varying depth of sector cut twisted tape inserts and variations in concentrations of hybrid nanofluids. This study finds application in design and thermal management of engines. The results revealed that, 9 mm sector cut twisted tape inserts with 0.05% concentration of hybrid nanofluids, the augment in heat transfer rate (HTR) by 51.22% higher. Furthermore, performance evaluation criteria (PEC) at higher values of Re number reached to be 2.67, 3.66, 4.598 with the insertion of 5 mm, 7 mm & 9 mm depths of sector twisted tape inserts with 0.05% concentration of hybrid nanofluids.

Keywords: Heat Exchanger, hybrid nanofluids, Nusselt number, performance evaluation criteria, friction factor

Cite this article as: Maheshbabu, P., Ramkrishnan, R., Reddy, G. S., & Jadhav, P. H. (2026). Flow dynamics behavior and thermal performance evaluation of double pipe counter flow heat exchanger with twisted tape inserts in the presence of hybrid nanofluids. Journal of Thermal Engineering, 12(6), 2116–2131. https://doi.org/10.47481/jten.0087

1. Introduction

In the present scenario, the energy efficiency of heat exchanger systems and increased industrial demand for higher heat transfer rate (HTR) need superior and economical heat transfer equipment. Many researchers have tried to improve the design of heat transfer equipment and enhance the heat transfer performance of working fluids [1]. The primary advantage of effective heat transfer lies in applications that require precise temperature regulation, such as automobile radiators, waste heat recovery (WHR), electrical equipment, chemical and food processing industries, battery heat dissipation, and microchannel heat sinks, as reported in detail in [2]. Many researchers have tried to boost heat transfer rate using baffles [3,4] extended surfaces [5] and porous media [6–11]. However, baffles, extended surfaces, and porous media lead to higher pressure drops. Therefore, to minimize the pressure drop, nanofluids could be an alternative method to achieve largest possible HTR with lower pressure drop. Furthermore, heat transfer enhancement and improvement in the efficacy of HEx systems through twisted inserts with nanofluids could be a better alternative solution, as reported in refs. [12,13]. Since twisted tape (TT) inserts create swirl flow, they act as swirl flow generators leading to a reduction in boundary layer thickness and as a result increased convective HTR as reported in Refs. [14] and [15]. Shehram et al. [16] investigated the thermal ef-

*Corresponding Author
E-mail Adress: jdvprakash@gmail.com

Submitted: 23 November 2025; **Accepted:** 23 February 2026

This paper was recommended for publication in revised form by Editor-in-Chief Ahmet Selim Dalkılıç

ficiency of solar flat plate collector channels accompanied by nanofluids. They reported that the Nusselt (Nu) number was maximum with the use of nanofluid compared to the base fluid water [17]. Esfe et al. [18] proposed a multi-objective optimization study of a HEx in the presence of MgO–water hybrid nanofluids (HNFs). They found that the total expense of the system was reduced by roughly 38% compared to the best-case scenario. Further, they noted that by using Al_2O_3 and Cu hybrid nanofluids [19] aluminum nitride nanofluids [20] and Cu–Al_2O_3/H_2O HNFs [21] the pumping power increased by around 3.3% and 3.88% at Re = 1000. Khargotra et al. [22], Li et al. [23], and Prasad et al. [24] explored a comprehensive analysis of CuO, Al_2O_3, and saturated carbon dioxide (SCO_2) nanofluid flows through a tube HEx with the insertion of TT. The results showed that at higher nanofluid concentrations, the friction factor (FF) increased by 1.29 times compared to base fluid water. Varma et al. [25] and Stalin et al. [26] saw the appearance of primary and secondary vortices with the positioning of TT inserts in a tube HEx. The insertion of TT may cause disruption of the boundary layer thickness near the tube wall, resulting in increased HTR. Further, Aghayari et al. [27] claimed that the heat transfer rate increased significantly with increasing twist ratio and concentration of HNFs, with marginal change in FF. Kumar et al. [28] reported that the maximum performance evaluation criteria (PEC) was found to be 1.74 at Re = 11,000 with a corresponding nanofluid concentration of 1.25% by volume. Recently, Mirzaei and Azimi [29] examined the use of 0.2% concentration of graphene oxide nanofluids and saw that the convective heat transfer coefficient was enhanced by 77% compared to the base fluid. In addition, at lower and higher values of Reynolds number, the HTR was enhanced by 18% and 24%, respectively, compared to baseline data reported in [30]. Further, Aruna and Niranjan [31] performed a numerical investigation using MHD micropolar HNFs and reported a considerable increase in HTR and friction resistance compared to the base fluid at higher Reynolds numbers. In recent studies, Narendran et al. [32] found that at a twist ratio (TR) of Y = 3, V-cut TT inserts enhanced the highest Nu number compared to square-cut inserts, at the cost of increased pressure drop. The V-cut TT inserts promoted the highest mixing of the fluid due to the formation of primary and secondary vortices. Further, the thermal enhancement ratio (THR) increased from 1.18 to 1.28 as the graphene nanofluid concentration changed from 0.02% to 0.12%, as reported in detail in [33]. Reddy et al. [34] explored the thermal performance factor (TPF) under the influence of W-cut TT inserts with variations in width ratio (WR) and depth ratio (DR) using CeO_2 nanofluids. They reported that higher WR and DR significantly enhanced the TPF at lower Reynolds numbers (Re = 2436), and then it reduced drastically at Re = 5513 [35]. Kumar et al. [36] and Murthy and Hegde [37] examined fluid flow behavior distributions with different configurations of V-cut TT inserts in the presence of nanofluids. They found that the Nu number increased from 1.32 to 2.59, 1.41 to 2.81, and 1.53 to 2.99 for solid TT, perforated TT, and V-cut perforated TT inserts, respectively. Kumar et al. [38] suggested that employing TT inserts with HNFs in a double pipe HEx (DPHEx) tube may effectively boost the thermal performance and number of transfer units (NTU) of the HEx. Atul Bhattad [39] performed an experimental study on HNFs (Al_2O_3/MgO) in a plate HEx and reported that the performance index reduced as the Reynolds number increased. On the other hand, the pumping power increased by 1.6% using HNFs compared to the base fluid.

Mund et al. [40] performed experimental and numerical investigations of a DPHEx using Al_2O_3/TiO_2 HNFs. They found that HNFs boosted the HTR significantly with a slight increase in pumping power. Ahmed et al. [41] examined HTR and pressure drop characteristics through a tube HEx in the presence of ZnO/TiO_2 binary HNFs. They discovered that the HTR increased by around 69% compared to the base fluid. Recently, plant et al. [42] and Singh and Sarkar [43] explored the hydrothermal characteristics of a HEx with V-cut TT inserts using HNFs. The study reported that higher DR and WR yielded largest HTR with a considerable increase in pressure drop. The V-cut TT inserts act as turbulators, promoting superior collisions between fluid molecules from the center to near the tube wall. Nevertheless, when HNFs were combined with V-cut TT inserts, the TPF increased from 1.33 to 1.37, as reported in Ref. [44]. Maheshbabu et al. [45] examined the efficiency of a tube HEx using hybrid nanofluids in a counter-flow heat exchanger. At higher concentrations of HNFs, the Nu number increased by 41.13% and 23.13% compared to the base fluid and lower concentrations of HNFs, respectively. Alhajaj et al. [46] performed experimental and numerical investigations of fluid flow behavior through a compact porous HEx in the presence of HNFs. The results showed that HTR improved significantly with the use of novel HNFs (CuO_2/Al_2O_3), along with a considerable increase in pressure drop. Since porous media obstruct fluid flow and increase inertia resistance, the pressure drops increase accordingly [47–50]. In addition, mixed convection heat transfer characteristics [51–57] and stability analysis of hybrid nanofluids have been performed. They reported that velocity decreases with the magnetic parameter but increases with the suction parameter, as detailed in [57,58]. Asokan et al. [59] reported that with the use of Al_2O_3/CuO HNFs, the average HTC and Nu increased by 7.2% and 6.7%, respectively, compared to the base fluid. This is because Al_2O_3/CuO HNFs enhance thermal conductivity and ensure proper dispersion of nanoparticles in the base fluid. Ramadhan et al. [60] and Bhattad and Sarkar [61] considered alumina–graphene HNFs with TT inserts for the enhancement of HTR. They found that higher WR and DR provided added rotation of fluid flow from the center to near the tube walls, resulting in thinner boundary layer thickness and, so, dissipation of a maximum amount of heat. Somasundaram and Pichumani [62] studied the flow dynamics and thermal performance of a shell-and-coil type HEx using spinel-type manganese ferrite–graphene oxide HNFs. They saw that the HTC increased by 14%, 8.79%, and 24.69% with the use of $MnFe_2O_4$/water magnetic nanofluids, GO/water nanofluids, and $MnFe_2O_4$–GO/water hybrid magnetic nanofluids, respectively, compared to base fluid water.

From the literature, the authors found that most studies have been performed using different types of nanofluids and HNFs. However, no researchers have investigated the use of sector-cut TT inserts in combination with ZnO/MWCNT/water-based HNFs. Additionally, the thermal performance and efficiency of thermal engineering equipment are adversely affected by high heat accumulation within the system. The use of water alone does not significantly enhance HTR due to its lower thermal conductivity. Therefore, to overcome these issues, ZnO/MWCNT/water-based HNFs are employed for the enhancement of HTR in various thermal engineering systems, including HEx, solar collectors, automobile radiators, and food processing industries. To improve the effectiveness and thermal efficacy of thermal systems, accumulated heat must be dissipated efficiently. Henceforth, the aim of the present study is to address the above knowledge gap by proposing the enhancement of HTR using variations in the depth of sector-cut TT inserts in the presence of ZnO/MWCNT/water-based HNFs. The advantage of sector-cut TT inserts is that they divert the fluid flow, promoting better mixing and thereby increasing the heat transfer coefficient. For the investigation, equal ratios of ZnO and MWCNT HNFs (50:50) are employed. The thermo-physical properties of the HNFs are reported in our earlier study [63]. A comprehensive analysis is carried out by considering three different depths of sector-cut TT inserts (5 mm, 7 mm, and 9 mm) and three different concentrations of ZnO/MWCNT HNFs (0.01%, 0.03%, and 0.05%), as reported in [63].

2. Experimental and numerical details

The experimental setup and twisted tape inserts used for the experimental investigations of CFHEx are shown in Figure 1 and Figure 2. The experimental setup consists of flow meters, hot and cold fluid tanks, a chiller tank, pumps, a U-tube manometer, and a bypass valve. The inner and outer tubes of the test section are composed of copper and mild steel, respectively. Table 1 presents the detailed specifications of the CFHEx according to Refs. [34,35]. To prevent heat loss from the test section, insulating asbestos material is placed over the outer tube. With the aid of a pump and flow control bypass valves, the arrangement is designed such that the heated fluid (hot water) passes through the annular zone, and the cold fluid (water or nanofluids) passes through the inner tube. Two flow meters are used to compute the mass flow rate (Reynolds number) of the hot and cold fluids. The Reynolds number of the working fluids (water/nanofluids) ranges from 2436 to 11626 (3 LPM to 15 LPM), while the hot fluid Reynolds number is kept constant (Re = 8322) on the annular side of the CFHEx. The experimental setup with sector-cut TT insert accommodation is shown in Figure 3. Aluminum strips of 1 m length and 15 mm width were used to fabricate the twisted tape inserts. Each strip was twisted uniformly to keep a constant twist ratio along its length. Additionally, a sector cut was introduced for every full twist to enhance fluid mixing and turbulence. The resulting inserts showed consistent helical geometry with periodic cuts, suitable for improving heat transfer in pipe flow applications. Figure 4 displays the specific dimensions of the TT insert implants. The water in the hot water tank is heated by a heater connected to the tank. The heated fluid circulates through the annulus and returns to the hot water tank outlet via a pump placed between the flow meter and the tank. The hot water tank stores the hot water returning from the HEx outlet. The cold fluid enters the tube through the flow meter, and the outlet cold fluid is collected by the chiller, which is kept at its first temperature. Insulation is added to the outer tube surface to reduce heat loss from the HEx. Thermocouples are embedded at the inlet and outlet of both tubes to measure the temperature. The mass flow rate is measured using flow meters positioned at the inlets of both pipelines. A U-tube differential manometer is adopted to measure the pressure drop of the cold fluid. The data is collected once the system achieves steady-state conditions. A bypass valve controls the flow rates of the hot and cold fluids. As soon as the temperatures of the hot and cold fluids reach steady-state conditions, the thermocouple readings are recorded at the outlets. Furthermore, uncertainties associated with different measuring instruments are also calculated. In comparison to the surface areas of the inner and outer tubes, the bent section area is quite small. Consequently, heat transfer in the bend zone section is neglected. The thermo-physical properties of the HNFs are considered for experimental and numerical investigations according to [63].

The ANSYS FLUENT 19.2 [64] software is employed to perform the numerical simulation as per Refs. [34,35]. An adiabatic boundary condition is assigned to the outer walls of the HEx. To improve the accuracy of the numerical simulation, the two-equation standard k–ε turbulence model is used according to Refs. [34,35]. A tetrahedral mesh is generated for numerical computations. The orthogonal quality of the tetrahedral mesh is kept at 0.8, and the skewness is kept below 0.8, with typical values around 0.1. High skewness can lead to convergence issues and inaccurate results; therefore, to avoid convergence issues, the tetrahedral mesh is kept below 0.8 for better accuracy. The convergence criteria are set at 10^{-5} for the momentum and continuity equations and 10^{-6} for the energy equation [34,35].

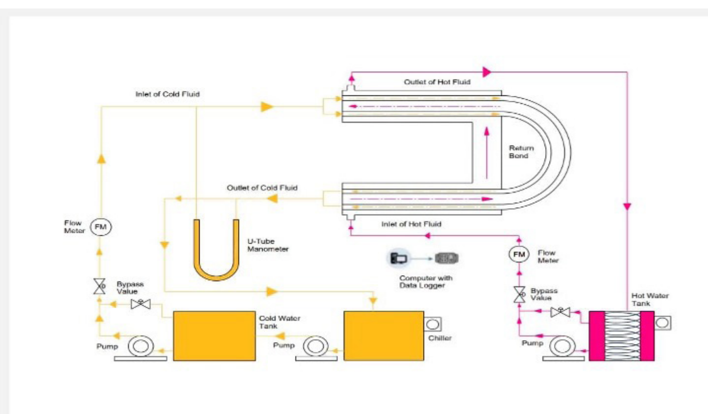

Figure 1. Schematic of experimental setup according to [34,35]

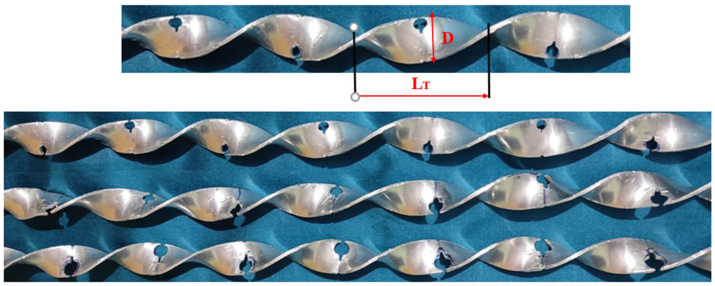

Figure 2. Twisted tape (TT) inserts used for experimental investigation

Table 1. Experimental setup specification ref. [34,35]

CFHEx	Values/Material
Tube length (mm)	2600
Entry temperature of hot fluid (°C)	60
Entry temperature of cold fluid (°C)	30
Outer tube OD (mm)	63
Inner tube ID (mm)	60
OD of outer tube (mm)	19
ID of inner tube (mm)	17
Outer tube	Mild steel
Inner tube	Copper

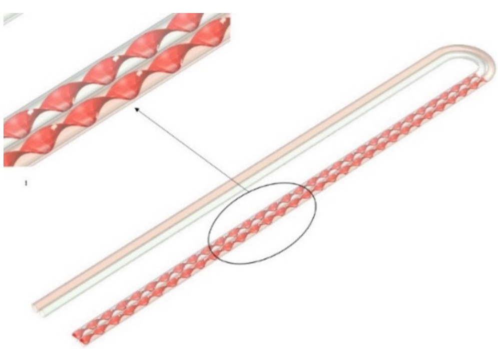

(a)

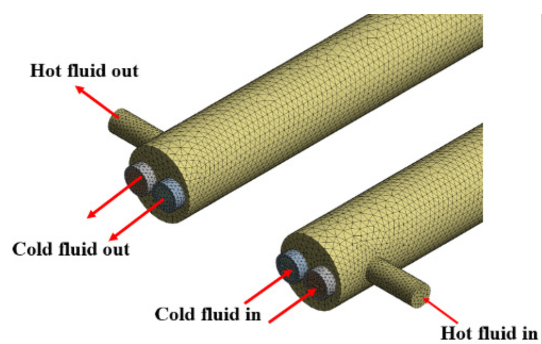

(b)

Figure 3. Modelling and meshing of TTCFHEx with inserts

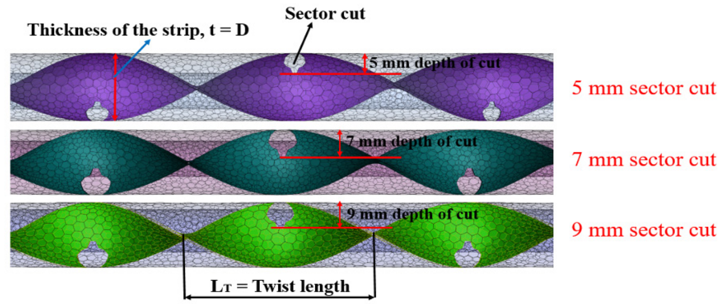

Figure 4. Inserts with varying depth of sector cuts TT inserts

2.1. Flow chart used the study

The systematic flow chart or clear schematic diagram shown in Figure 5, outlining the key steps and logical simulation setup and its integration with the experimental used for work presented below.

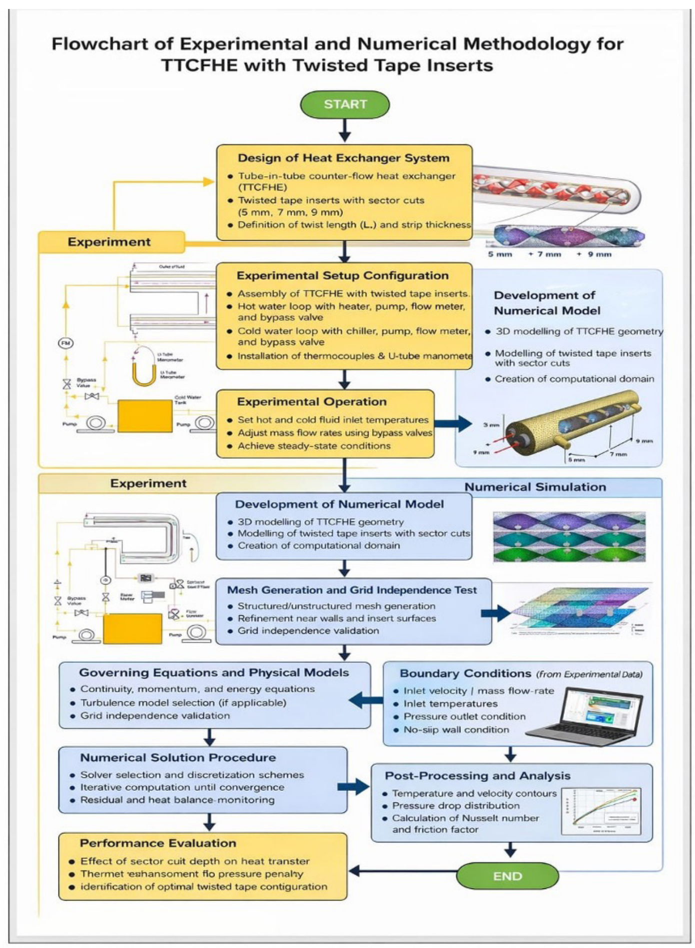

Figure 5. Systematic flow chart diagram

2.3. Governing equations used for numerical study

The governing equations (1) – (7) are employed for the numerical computations are as follows as per ref. [65]:

The conservation of mass for an incompressible flow is expressed by the continuity equation,

$$\frac{\partial\ (\rho u_i)}{\partial\ x_i} = 0 \tag{1}$$

Where, ρ denotes the fluid density and is the time-averaged velocity part.

The Reynolds-averaged momentum equation is written as:

$$\rho \overline{u}_j \frac{\partial\ \overline{u}_i}{\partial\ x_j} = -\frac{\partial\ \overline{p}}{\partial\ x_i} + \frac{\partial}{\partial\ x_j}\left[(\mu + \mu_t)\left(\frac{\partial\ \overline{u}_i}{\partial\ x_j} + \frac{\partial\ \overline{u}_j}{\partial\ x_i}\right)\right]$$

Where, $\overline{p}$ is the mean pressure, μ_t is the molecular dynamic viscosity, and $\mu_t = \rho C_\mu \frac{k^2}{\varepsilon}$ is the turbulent (eddy) viscosity. The turbulent viscosity is defined as:

$$\mu_t = \rho C_\mu \frac{k^2}{\varepsilon} \tag{3}$$

The transport of thermal energy equation is written as:

$$\rho \overline{u}_j \frac{\partial\ \overline{T}}{\partial\ x_j} = \frac{\partial}{\partial\ x_j}\left[(\alpha + \alpha_t)\left(\frac{\partial\ \overline{T}}{\partial\ x_j}\right)\right] \tag{4}$$

Where, $\overline{T}$ is the mean temperature, C_p is the thermal conductivity of the base fluid, Pr_t is the specific heat at constant pressure, and denotes the turbulent Prandtl number. Where, $\alpha_t = \frac{k_f}{\rho C_p}$ is molecular thermal diffusivity and $\alpha_t = \frac{\mu_t}{\rho Pr_t}$ is the turbulent thermal diffusivity.

The transport equation for the turbulent kinetic energy k is given by

$$\rho \overline{u}_j \frac{\partial\ k}{\partial\ x_j} = \frac{\partial}{\partial\ x_j}\left[\left(\mu + \frac{\mu_t}{\sigma_k}\right)\left(\frac{\partial\ k}{\partial\ x_j}\right)\right] + P_k - \rho\varepsilon \tag{5}$$

Where, P_k is the production of turbulent kinetic energy and ε is the turbulent dissipation rate. The production term P_k is defined as:

$$P_k = \mu_t \left(\frac{\partial\ \overline{u}_i}{\partial\ x_j} + \frac{\partial\ \overline{u}_j}{\partial\ x_i}\right)\frac{\partial\ \overline{u}_i}{\partial\ x_j} \tag{6}$$

The transport equation for the turbulent dissipation rate ε is expressed as:

$$\rho \overline{u}_j \frac{\partial\ \varepsilon}{\partial\ x_j} = \frac{\partial}{\partial\ x_j}\left[\left(\mu + \frac{\mu_t}{\sigma_\varepsilon}\right)\left(\frac{\partial\ \varepsilon}{\partial\ x_j}\right)\right] + C_{\varepsilon 1}\frac{\varepsilon}{k}P_k - C_{\varepsilon 2}\rho\frac{\varepsilon^2}{k} \tag{7}$$

Where, $C_{\varepsilon 1}$ and $C_{\varepsilon 2}$ are empirical model constants. The standard k–ε model constants employed in the present study are $C_\mu = 0.09, C_{\varepsilon 1} = 1.44, C_{\varepsilon 2} = 1.92, \sigma_k = 1.0, \sigma_\varepsilon = 1.3$.

For experimental and numerical investigations, the thermo-physical properties are computed using Equations (8) – (18). The effective properties of ZnO/water nanofluids and MWCNT/water nanofluids computed using Equation (8) per ref. [66].

$$\rho_{nf} = \varphi_p \rho_p + (1 - \varphi_p)\rho_{bf} \tag{8}$$

The density of hybrid nanofluids (HNF) is computed using Equation (9) per [67].

$$\rho_{HNF} = \varphi_{ZnO}\rho_{ZnO} + \varphi_{MWCNT}\rho_{MWCNT} + (1 - \varphi)\rho_{bf} \tag{9}$$

φ denotes total volume concentration of two dissimilar types of nanoparticles dispersed HNF is computed using Equation (10) as per [67].

$$\varphi = \varphi_{ZnO} + \varphi_{MWCNT} \tag{10}$$

The effective viscosity of nanofluids is computed using the Equation (11) as per [66].

$$\mu_{nf} = (1 + K_\mu \varphi)\mu_{bf} \tag{11}$$

Where $K_\mu = 2.5$.

Brinkman model [67] presents Equation (12).

$$\mu_{nf} = \frac{\mu_{bf}}{(1 - \varphi)^{2.5}} \tag{12}$$

Batchelor model [67] presents Equation (13).

$$\mu_{nf} = (1 + K_1\varphi + K_2\varphi^2)\mu_{bf} \tag{13}$$

Where, K_1 is constant and is equal to 2.5 and K_2 defines deviation from very dilute limit of suspension, which is allowing superimposed Brownian motion, hence coefficient K_2 value is computed as per [67]. The effective specific heat capacity of nanofluids can be determined using the Equation (14) per ref. [66].

$$C_{p_{nf}} = \frac{\varphi_p \rho_p C_{p_p} + (1 - \varphi_p)\rho_{bf} C_{p_{bf}}}{\rho_{nf}} \tag{14}$$

According to Equation (13), specific heat capacity of HNF can be evaluated using Equation (15) as per [67].

$$C_{p_{HNF}} = \frac{\varphi_{ZnO}\rho_{ZnO} C_{p_{ZnO}} + \varphi_{MWCNT}\rho_{MWCNT} C_{p_{MWCNT}} + (1 - \varphi)\rho_{bf} C_{p_{bf}}}{\rho_{HNF}} \tag{15}$$

The effective thermal conductivity of nanofluids is computed using the relation (16) as per [67].

$$k_{nf} = \frac{k_p + (n - 1)k_{bf} - (n - 1)\varphi_p(k_{bf} - k_p)}{k_p + (n - 1)k_{bf} + \varphi_p(k_{bf} - k_p)} \tag{16}$$

Where, n denotes empirical shape factors to consider the influence of particles shape varied from 0.5 to 0.6 detailed in [67]. The n is given as 3/ψ, where ψ denotes particle sphericity, which is defined as ratio of surface area of sphere to the surface area of particles. Therefore, spherical nanoparticles n = 3. In such case Hamilton and

Crosser model (n = 3) is similar as Maxwell model [67] as follows in Equation (17):

$$\frac{k_{nf}}{k_{bf}} = \frac{k_p + 2k_{bf} - 2\varphi_p(k_{bf} - k_p)}{k_p + 2k_{bf} + 2\varphi_p(k_{bf} - k_p)} \quad (17)$$

The effective conductivity of HNFs is defined as per Maxwell model should be considered as Equation [18].

$$\frac{k_{nf}}{k_{bf}} = (\frac{(\varphi_{ZnO}k_{ZnO} + \varphi_{MWCNT}k_{MWCNT})}{\varphi} + 2k_{bf} + 2(\varphi_{ZnO}k_{ZnO} + \varphi_{MWCNT}k_{MWCNT} - 2\varphi k_{bf}) \times (\frac{(\varphi_{ZnO}k_{ZnO} + \varphi_{MWCNT}k_{MWCNT})}{\varphi} + 2k_{bf} - (\varphi_{ZnO}k_{ZnO} + \varphi_{MWCNT}k_{MWCNT}) + 2\varphi k_{bf})^{-1} \quad (18)$$

3. Boundary conditions, uncertainty and data reduction analysis

For numerical investigations, uniform velocity boundary conditions are kept at inlet of tube. At the inlet of tube; cold fluid Re number is varied from 2436 to 11626 while that of hot fluid Re number is maintained constant according to [34, 35]. The cold fluid inlet temperature is maintained at 30 °C while hot fluid temperature is maintained at 60 °C according to refs. [34, 35]. No-slip boundary condition is used near the tube wall and shell side walls. The cold fluid flow inside the tube wall is maintained a diathermic wall whereas annulus or shell side wall is maintained adiabatic condition as per [34, 35].

The uncertainty analysis is performed according to the ref. [68].The computed errors present in the experimental study are discussed and reported in the current section. The errors and ambiguities present in the experimental studies are discussed in detail. The uncertainty in velocity, temperature and manometer readings is found to be ± 1.25%, ± 1.2% and ±1.15%, respectively. Further, uncertainty due to voltage variations and rotameter are computed and are found to be ± 0.6% and ±1.2%, respectively. The details of uncertainty analysis can be found in our previous work ref. [34].

The Equations (19) and (20) are employed to examine the heat transfer rate between hot fluid Q_h (water) and cold fluid Q_c . Assuming that, the amount of heat transferred by the hot fluid is gained by the cold HNFs nanofluids according to ref. [34, 35].

$$Q_h = \dot{m}C_{p,h}(T_{h,i} - T_{h,o}) \quad (19)$$

$$Q_c = \dot{m}C_{p,c}(T_{c,o} - T_{c,i}) \quad (20)$$

The mean heat transfer rate among hot and cold fluids are examined using Equations (21) & (22).

$$Q_{avg} = \frac{Q_c + Q_h}{2} \quad (21)$$

$$Q_{avg} = U_i A_i \Delta T_{LMTD} \quad (22)$$

Where, A_i, ΔT_{LMTD} is area of HEx and log, mean temperature difference which are calculated using the Equations (23) & (24).

$$A_i = \pi d_i L \quad (23)$$

$$\Delta T_{LMTD} = \frac{(\Delta T_1 - \Delta T_2)}{\ln\left(\frac{\Delta T_1}{\Delta T_2}\right)} \quad (24)$$

Where, ΔT_1 and ΔT_2 denotes inlet temperature & outlet temperature difference between hot and cold fluids respectively and are computed using Equation (25).

$$\Delta T_1 = (T_{h,i} - T_{c,o})$$

$$\Delta T_2 = (T_{h,o} - T_{c,i}) \quad (25)$$

The OHTC computed using the relations (26) and (27).

$$U_i = \frac{Q_{avg}}{A_i \Delta T_{LMTD}} \quad (26)$$

The U_i is calculated using Equation (27).

$$\frac{1}{U_i} = \frac{1}{h_i} + B \quad (27)$$

Where, h_i is HTC and is constant and which is computed with account of Wilson chart according to ref. [68].

The Nu number is evaluated using the Equation (28).

$$Nu = \frac{h_i d_i}{K_f} \quad (28)$$

The FF computed using the Equation (29).

$$f = \frac{\Delta P}{\frac{L}{d_i}\left(\frac{\rho V^2}{2}\right)} \quad (29)$$

The PEC signifies the performance of HEx. The PEC is evaluated with the Equation (30) as per [34,35].

$$PEC = \frac{\left(\frac{Nu_{HNF}}{Nu_{BFW}}\right)}{\left(\frac{f_{HNF}}{f_{BFW}}\right)^{1/3}} \quad (30)$$

4. Result and discussion

4.1. Validation study

Experimental and numerical investigations are performed using water as the base fluid over a wide range of Reynolds numbers. The results of the friction factor (FF) values are compared with the correlation provided by Petukhov [69], as shown in Figure 6. The figure proves good agreement between both the experimental and numerical results and the Petukhov correlation [69]. The deviations of the experimental and numerical FF values from the Petukhov correlation are found to be less than 5.19% and 2.36%, respectively. The slightly higher deviation seen in the experimental results compared to the numerical study is likely due to uncertainties inherent in the experimental measurements. Additionally, the deviation between the present experimental and numerical FF results is found to be 2.77%, which is well within an acceptable range.

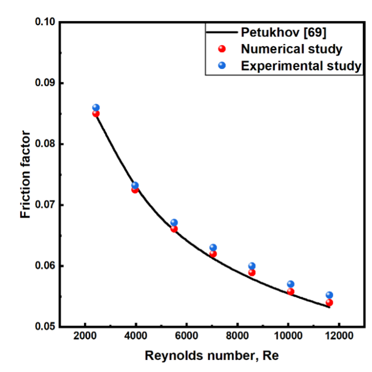

Figure 6. Comparative study of friction factors with Petukhov [69] [Figure 5. Reference temperature for heat transfer (a) and friction (b) calculations by Deissler's method for fluids with variable viscosity. Key: solid line, heating of fluid; dashed line, cooling of Ruid.]. Reproduced from Ref. [69] with permission from [Elsevier], © [1970]

4.2. Grid independence test

To decide the ideal/best grid size, a grid/mesh independence test is conducted for five different grid sizes: 1,825,301; 2,014,705; 3,247,855; 4,702,214; and 6,088,741. For the grid sensitivity analysis, the base fluid water is used. The grid sensitivity analysis is performed for the cold fluid at a Reynolds number of 3978. For the corresponding cold fluid condition, the outlet temperature of the tube is measured and reported in Table 2. The temperature deviation is computed based on the largest grid size of 6,088,741. The grid test study shows that the grid size of 4,702,214 shows the least deviation in outlet temperature, which is about 0.25% when compared to the other grid sizes of 1,825,301; 2,014,705; and 3,247,855. Therefore, for further numerical investigations, the grid size of 4,702,214 is used for numerical computations.

Table 2. Grid independence examination results

Sr. No.	No. of elements	Outlet temperature of tube (°C)	Deviation (%)
1	1825301	33.79	5.06
2	2014705	34.05	4.33
3	3247855	34.75	2.36
4	4702214	35.50	0.25
5	6088741	35.59	Base line data

4.3. Comparative study of heat transfer rate (HTR)

HTR is computed using Equation (21). Figure 7 explores the changes in HTR with Reynolds number for distinct concentrations of HNFs and the base fluid water (BFW). From the figure, it is clearly seen that in the presence of HNFs, HTR increases significantly when compared to BFW. Also, with increasing concentrations of HNFs, the HTR increases considerably compared to lower concentrations and is significantly higher in comparison to BFW. The addition of HNFs to BFW enhances the thermal conductivity of the fluid. Moreover, significant energy exchange between the hot and cold fluids takes place, and this mechanism is referred to as chaotic movement. At higher Reynolds numbers, effective momentum of the fluid flow increases; as a result, the residence time available to absorb heat is minimum. The average increase in HTR of 0.05%, 0.03%, and 0.01% concentrations of HNFs is found to be 40.71%, 34.24%, and 21.28%, and 38.86%, 32.64%, and 20.25% higher than that of BFW for numerical and experimental computations, respectively. It is also noteworthy that for the 0.05% concentration of HNFs, the average HTR improved by 16.06% and 4.83%, and 15.47% and 4.71% compared to the 0.01% and 0.03% concentrations of HNFs for numerical and experimental investigations, respectively. Henceforth, for further investigations, only the 0.05% concentration of HNFs with sector-cut TT inserts is considered.

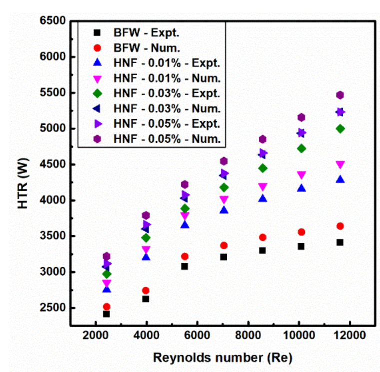

Figure 7. Comparative study of HTR for BFW and various concentration of HNFs

4.4. Velocity contours and velocity streamlines

Figure 8 presents velocity contour plots at higher Reynolds numbers with a 0.05% concentration of HNFs. The flow inside the tube is kept in the turbulent regime. Except for the tube inlet region (neglected length), the velocity in the plain tube heat exchanger stays relatively constant. However, when the fluid passes through the tube with twisted tape inserts, the flow is diverted due to the presence of the inserts. This causes the fluid particles to rotate around the inserts, generating a swirling flow motion. The swirl enhances fluid mixing near the tube wall, thereby disrupting the boundary layer thickness. Additionally, sector-cut twisted tape inserts promote the formation of secondary vortex flows [34,35]. The combination of the primary vortex created by the twisted tape and the secondary vortices generated by the sector cuts increases the turbulent intensity of the flow, resulting in the formation of a thinner boundary layer near the tube wall. This thinner boundary layer improves the heat dissipation rate. Moreover, the swirling motion effectively mixes the fluid near the pipe wall, reduces the velocity gradient, and significantly enhances the heat transfer rate as detailed in [32] and [34,35].

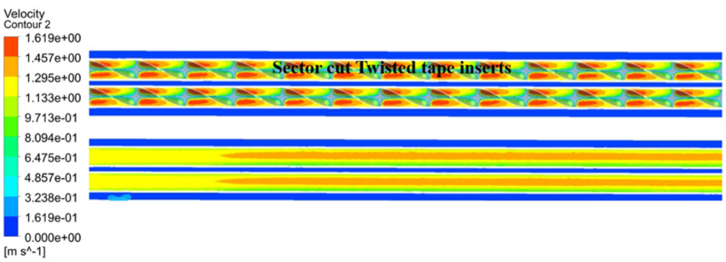

Figure 8. Velocity contour at Re = 11626 for 0.05% concentration of HNFs with and without inserts

Figure 9 illustrates the changes in axial velocity along the z-direction for a plain tube (PT) and tubes fitted with sector-cut twisted tape (TT) inserts with varying depths of cuts, using a 0.05% concentration of HNFs at higher Reynolds numbers (Re). From the figure, the axial velocity in the plain tube shows minimal variation. However, with the introduction of sector-cut TT inserts, the fluid flow begins to deviate from a purely axial direction, generating a swirling motion. As the depth of the cut increases, the intensity of the swirl flow also increases, leading to enhanced fluid mixing, as referred to in [34,35].

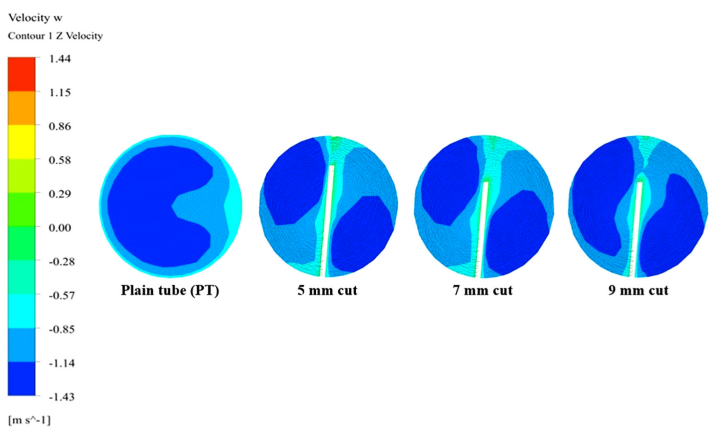

Figure 9. Velocity variation at Re = 11626 and 0.05% HNFs for various depths of cuts

Figure 10, depicts the velocity streamlines along the length of the heat exchanger tube at Re = 11,626 with a 0.05% concentration of ZnO/MWCNT HNFs and sector-cut TT inserts of depths 5 mm, 7 mm, and 9 mm. Figure 10a, shows the velocity streamlines for the 5 mm sector-cut TT inserts with a maximum velocity of 1.644 m/s. It is clearly seen that the insertion of TT inserts causes the flow direction to shift from purely axial flow to swirl flow motion. The streamlines flowing around the TT inserts generate the primary swirl flow [32]. Additionally, the consecutive cuts located at the crest and trough of the TT inserts create bypass secondary swirl flow motion. The interaction of these primary and secondary vortices enhances fluid mixing, thereby increasing the turbulent intensity of the flow and improving the heat transfer rate [32]. Furthermore, as the sector-cut depth increases (Figures 10b and 10c), fluid mixing improves further, leading to a reduction in the boundary layer thickness near the wall, which enhances the heat transfer rate.

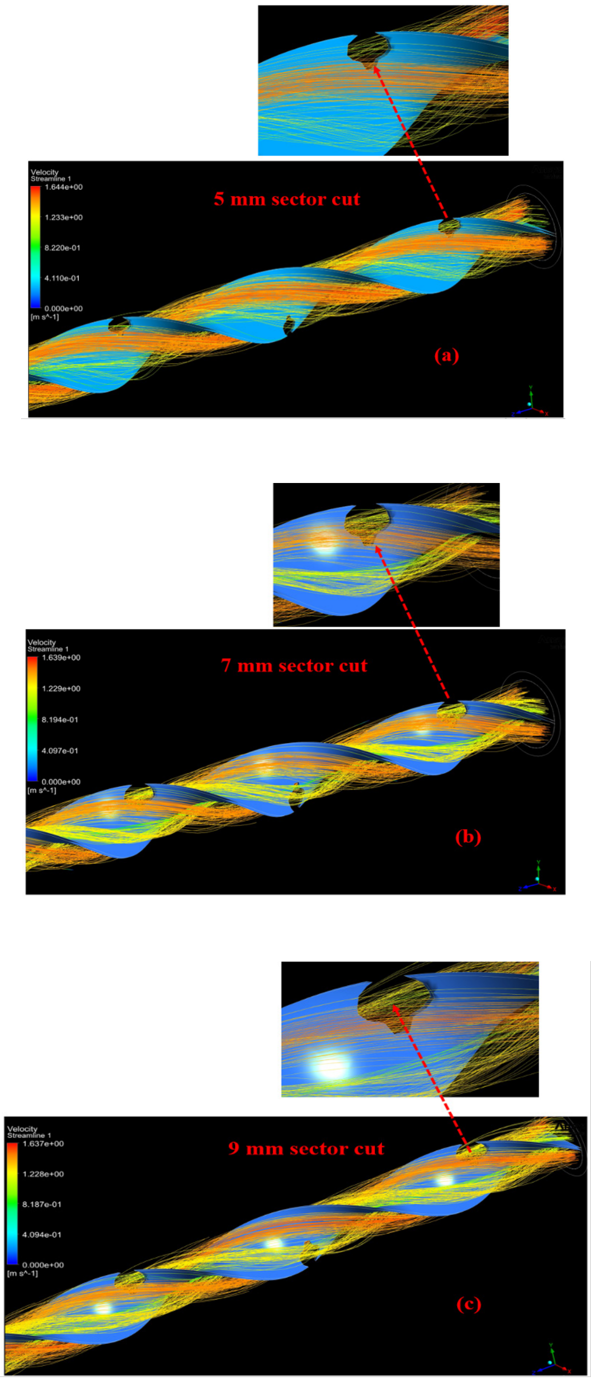

Figure 10. Velocity streamlines at Re = 11626 and 0.05% HNFs for, a) 5 mm, b) 7 mm and c) 9 mm depth of cuts

4.5. Heat transfer rate (HTR)

Figure 11 proves the heat transfer rate (HTR) for a plain tube (PT) and a tube with various depths of sector-cut twisted tape (TT) inserts with respect to Reynolds number (Re). From the figure, it is seen that the HTR increases significantly with increasing Re number for both the PT and the tube with TT inserts. The HTR results show marginally similar trends for both the experimental and numerical investigations when base fluid water (BFW) is considered. However, in the presence of hybrid nanofluids (HNFs), a significant enhancement in HTR is seen compared to BFW. Since hybrid nanoparticles blended with BFW enhance the thermal conductivity of the fluid, this leads to an improvement in HTR. Also, due to the movement of hybrid nanoparticles in the base fluid water (BFW), a continuous exchange of energy takes place between the cold and hot fluids. Further, upon introducing various depths of sector-cut TT inserts in the heat exchanger tube, the HTR increases significantly compared to BFW, and it also increases monotonically compared to HNFs without TT inserts. Additionally, as the TT sector-cut depth increases, the HTR also increases meaningfully and marginally relative to BFW and HNFs without TT inserts. The sector-cut TT inserts act as turbulence promoters, leading to an increased level of turbulence within the flow and contributing to an improved heat transfer rate. In addition, increasing the depth of sector-cut TT inserts may induce a primary vortex near the twisted tape and a secondary vortex behind the cuts, causing a swirl flow motion that results in enhanced fluid mixing [34, 35]. In general, the complete length of sector-cut TT inserts induces continuous swirling flow motion within the heat exchanger tube for: (a) increasing the residence time of fluid flow, (b) reducing the thermal boundary layer thickness near the tube walls, and (c) enhancing fluid mixing between the core flow and the tube walls [15]. The augmentation in HTR in the presence of HNFs is found to be 38.86% and 40.71% higher compared to PT with BFW for numerical and experimental investigations, respectively. In addition, for 5 mm, 7 mm, and 9 mm depths of sector-cut TT inserts with HNFs, the augmentation in average HTR is found to be 46.28%, 51.92%, and 54.23% (numerical) and 44.03%, 49.47%, and 51.22% (experimental) higher than PT with BFW. Also, the discrepancy between the experimental and numerical results of HTR is found to be around 5.34% for the plain tube with BFW.

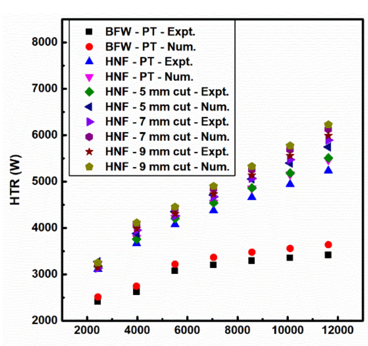

Figure 11. HTR for BFW PT and HNFs with various depths of cut inserts

4.6. Overall heat transfer coefficient (OHTC)

The overall heat transfer coefficient (OHTC) is evaluated using Equation (26). Figure 12 explores the results of OHTC for a plain tube (PT) with BFW, HNFs, and HNFs with 5 mm, 7 mm, and 9 mm depths of sector-cut TT inserts. The OHTC is the lowest for PT with BFW, and it increases with increasing depth of sector-cut TT inserts in the presence of HNFs. Since the heat exchange between the hot and cold fluid is least for PT with BFW due less thermal conductivity. However, in the presence of HNFs, the OHTC increases considerably and progressively with increasing number of Reynolds. This is because the addition of HNFs to BFW improves the thermal conductivity of the fluid, thereby enhancing heat exchange between the cold and hot fluids. The average increase in OHTC is found to be 56.91% and 55.08% higher for HNFs compared to BFW over the range of Reynolds numbers studied. Consequently, the OHTC is found to be significantly higher in the presence of HNFs with TT inserts. In addition, with increasing depth of sector-cut TT inserts, the OHTC increases further. This is because sector-cut TT inserts change the flow direction of the fluid, leading to vortex formation. The formation of vortices depends on the depth of the sector-cut TT inserts. Therefore, a greater depth of cuts results in stronger vortex formation, which enhances mixing of the fluid between the core region and the tube wall [34, 35]. The numerical study shows that with the insertion of 5 mm, 7 mm, and 9 mm depths of sector-cut inserts, the average increase in OHTC is 64.14%, 73.07%, and 76.57%, respectively, compared to PT with BFW over the studied range of Reynolds numbers. Further, at a higher sector-cut depth (i.e., 9 mm) of TT inserts, the average increase in OHTC is found to be 13.93% higher than that of HNFs with PT.

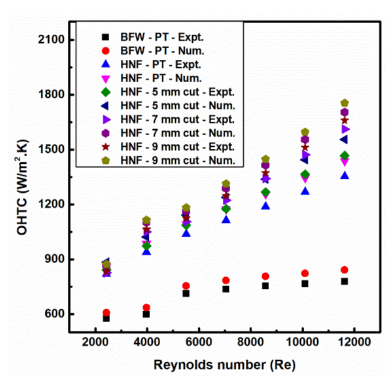

Figure. 12. OHTC for BFW PT and HNFs with various depths of cut inserts

4.7. Heat transfer coefficient (HTC)

Figure 13 illustrates the HTC variations for PT with BFW and HNFs and HNFs with various depth of sector cut TT inserts with respect to Re number. The result of HTC shows more or less similar results for both experimental and numerical investigations are performed. However, the discrepancy between experimental and numerical studies is found to be 9.57%. Furthermore, PT with HNFs shows significant enhancement in HTC and further it increases with increasing the Re number. This is because the surface area and random collision between the hybrid nanoparticles increases. Also, at higher values of Re number; effective momentum of fluid is forcible to flow that shows the temperature difference between hot and cold fluid reduces more effectively as a result increase in HTC [34, 35] and [45]. The average increase in HTC is found to be 133.99% and 140.87% higher in the presence of HNFs when compared to PT with BFW for both experimental and numerical investigations are considered. Furthermore, HNFs with TT inserts in a tube HEx shows a greater augment in the HTC. Since, with insertion of TT inserts changes the flow direction of fluid from axial flow to radial flow that leads to formation of vortex generators. This vortex generator helps in correct mixing of fluid in the core region near the tube wall that encourages the augment in HTC. Further, at higher values of Re number with TT inserts; increases the turbulent intensity and formation of vortex generator [34, 35]. In addition, with increasing depth of sector cut TT inserts; HTC increases considerably. Since, at higher depth of cuts disruption of boundary layer thickness due to primary vortex and secondary swirl flow motion. It is also noted that, with insertion of 5 mm, 7 mm and 9 mm depth of sector cut TT inserts; the average increase in HTC is found to be 195.04%, 271.38% and 305.78% higher than that of PT with BFW, respectively.

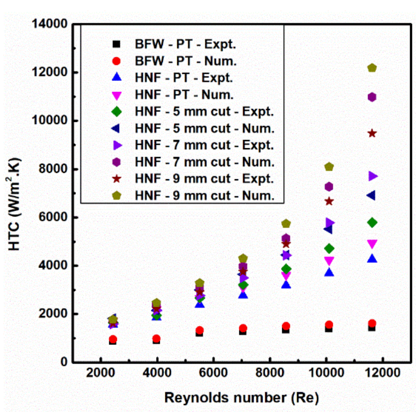

Figure 13. HTC results for BFW PT and HNFs with various depths of cut inserts

4.8. Nusselt number (Nu)

The Nu number is computed using the relation (28). Figure 14 presents the experimental and numerical analysis of Nu number for PT and tubes with sector-cut TT inserts with respect to flow Re number. The results show that the Nu number increases steadily with increasing Re number for both the base fluid and HNFs. The experimental and numerical results of Nu number is found to be very similar for the PT without TT inserts. However, the deviation between the experimental and numerical results reached 9.6% with use of BFW. Subsequently, Nu number with 9 mm depth of sector cut shows significantly higher when compared to 3 mm, 5 mm sector cut and PT without TT inserts. This is attributed to the increase in turbulence generated by the deeper depth of sector cut TT inserts within the heat exchanger tube, that enhances the fluid mixing resulted in increase in the Nu number. Also, higher concentration of HNFs nano fluids improves thermal conductivity of fluids. Specifically, the insertion of 9 mm depth of sector-cut TT inserts results in an enhancement of the Nu number by 89.92%, 41.34%, and 17.6% when compared to PT with BFW, 5 mm cut, and 7 mm cut TT inserts, respectively. Similar tendency has been seen in the literatures [34,35] and [45].

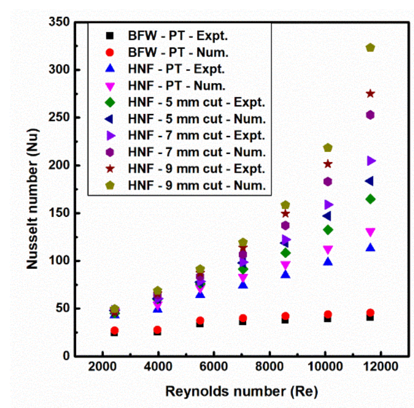

Figure 14. Results of Nu number for BFW PT and HNFs with various depth of cut inserts

The presents work results are compared with the earlier study of literature [34]. In the earlier study the authors [34] have considered the same experimental setup and the same numerical domain with cerium oxide nanofluid. Figure 15 presents comparative results of Nu number with respect to flow Re number. The result of Nu number increases with increasing flow Re number as well as increases with increasing the depths of sector cut of twisted tape inserts. However, when compared to ref. [34] the Nu number showed significantly higher for higher depths of sector cut TT inserts. The insertion of 5 mm, 7 mm and 9 mm depths of sector cut TT inserts; the average increase in Nu number is attained to be 17.69%, 33.65% and 24.57% higher when compared to WR = 4/15 and DR = 2/15, WR = 8/15 and 4/15, WR = 12/15 and 6/15, respectively in the range of Re number is simulated. This is because, HNFs attains the higher thermal conductivity than that of cerium oxide nanofluid. Also, this is attributed to the increase in turbulence generated by the deeper depths of sector cut within the heat exchanger tube, that enhances the fluid mixing resulted in the Nu number. Also, higher concentration of HNFs nano fluids improves thermal conductivity of fluids. Therefore, from the study it confirms that the HNFs with different depths of sector cut TT inserts has significant impact on the HTR when compared to cerium oxide nanofluid of literature [34].

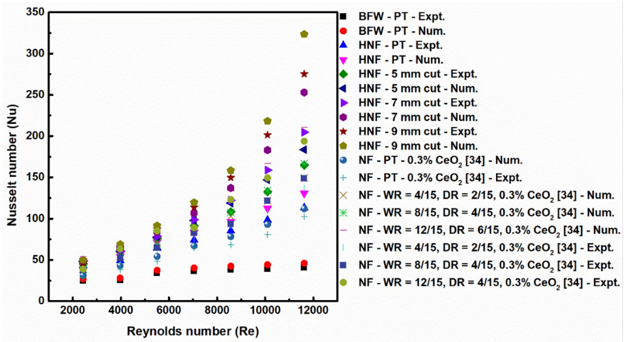

Figure 15. Comparative study of Nu Number [Figure 11. Comparative results of Nu versus Re for water and nanofluid.]. Reproduced from Ref. [34] with permission from [Taylor and Francis], © [2025]

4.9. Friction factor (FF)

The friction factor is evaluated using the relation (29). Figure 16 illustrates the variations of FF with Re number for PT tube with and without TT inserts. The friction resistance shows significantly less for the PT with BFW. Further, FF result is found to be marginally very similar for the HNFs with PT. However, FF result increases marginally for PT in the presence of HNFs. Since hybrid nanoparticles blend with BFW intensify the viscosity of fluid that allows resistance to flow of the fluid. In addition, HNFs with higher depth of cut sector inserts have higher friction resistance. Because a higher depth of sector cut allows the fluid to recirculate slightly behind the cuts that leads to increase the fluid turbulence and which is contributing to a higher-pressure drop. Nonetheless, the friction resistance is exactly proportional to the pressure drop factor. On the other hand, higher concentrations of nanofluids intensify added frictional resistance owing to the greater viscosity due to addition of hybrid nanoparticles. Further, highly viscous hybrid nano-solid particles owing to increase pressure drop due to increase in shear stresses amongst the solid particles and BFW [70]dispersion stability and application at higher temperatures are among the challenges that must be overcome. In this work, a new class of stable hybrid nanofluid based on multi-walled carbon nanotube (MWCNT. Additionally, greater surface area is available for the fluid to take part with TT inserts that could increase fluid friction.

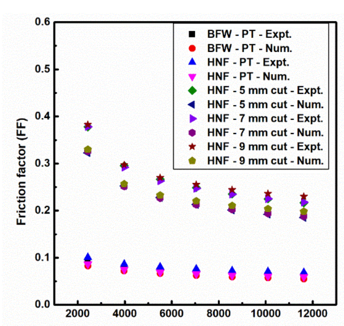

Figure 16. FF results for BFW PT and HNFs with various depths of cut inserts

4.10. Performance evaluation criteria (PEC)

The PEC is defined as the ratio of heat transfer enhancement ratio to one third of pumping power [71]. The PEC is computed using the Equation (30). Figure 17 examined the PEC variations for HNFs with different depth of sector cut TT inserts with respect to Re number. From the figure, PEC shows greater than 1 for all depth of sector cut TT inserts. The PEC shows the lowest value for lower values of Re number, and it increases progressively with increasing Re number. In addition, PEC values are found to be 1.17, 1.12, 1.16 and 2.67, 3.66, 4.598 for 5 mm, 7 mm and 9 mm sector cut TT inserts at lower and higher values of Re number, respectively. However, PEC increases with increasing Re number and showed maximum for 9 mm depth of sector cut TT inserts. This is due to that, 9 mm sector cut TT inserts provides higher enhancement ratio with very marginally increasing friction resistance relatively to 5 mm and 3 mm sector cut TT inserts. From numerical investigations, with insertion of 9 mm depth of sector cut TT inserts, the average augment in PEC is found to be 33.45% and 14.92% higher than that of 5 mm and 3 mm depth of cut TT inserts, respectively.

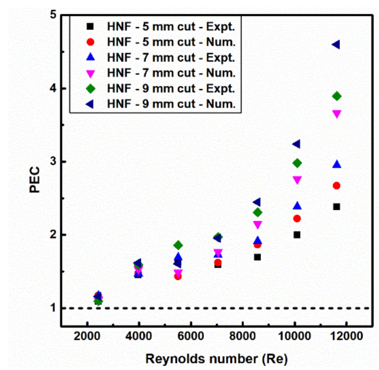

Figure 17. PEC results in HNFs with various depths of cut inserts

5. Conclusion

The aim of this study is to analyse the performance of CFHEx combined with ZnO/MWCNT hybrid nanofluids (HNFs) using sector TT inserts. Experimental and numerical analyses were performed for different concentration of HNFs and various depths of sector cut TT inserts. The Reynolds number of the cold fluid ranged from 2436 to 11,626, while the Reynolds number of the hot fluid stays constant. The important following key findings are mentioned below:

- The integration of sector cut TT geometry in a tube HEx induces the primary and secondary vortex flows has a significant impact on the flow dynamics. The primary vortex induced by the TT introduces a swirling or helical flow pattern which promotes strong tangential velocity components in the fluid. Meanwhile, the secondary vortex formed due to the sector cuts or edge modifications introduces localized turbulence and added mixing zones within the flow.
- The combined vortices disrupt the boundary layer thickness particularly near the tube wall region. A thinner

boundary layer reduces thermal resistance between the wall and the fluid allowing more efficient heat transfer from the wall to the flowing medium. The swirling and secondary flows continuously move higher-temperature fluid from the tube wall to the core and colder fluid from core to the wall.

- Additionally, the reduction in velocity gradient near the wall due to enhanced mixing minimizes the stagnant region of flow next to the wall. This causes a more uniform velocity distribution and improves momentum exchange, which also positively affects heat transfer.
- The significant augment in HTR is seen with the implementation of TT inserts with 5 mm, 7 mm, and 9 mm sector cut TT inserts, in combination with ZnO/MWCNT HNFs. The average HTR is seen to increase by 46.28%, 51.92%, and 54.23% with numerical and 44.03%, 49.47%, and 51.22% with experimental when compared to PT with BFW, respectively. However, it is also seen that this combination led to increased frictional resistance, particularly at higher depths of sector cuts TT inserts.
- The use of higher depth sector-cut inserts (9 mm) consistently led to maximum Nusselt number values among all tested configurations. The 9 mm sector cut TT inserts with HNFs showed an average increase in Nu numbers of 41.34% and 17.6% compared to 5 mm and 7 mm TT inserts, respectively.
- The PEC value for all tested configurations of sector-cut inserts yields greater than 1 that confirms thermohydraulic improvement. The 9 mm sector cut insert achieved the highest PEC of 4.598 at the largest Reynolds number that shows best performance under high flow conditions.
- The use of hybrid nanofluids in conjunction with sector-cut twisted tape inserts significantly enhances the heat transfer rate compared to conventional fluids and plain tube configurations. The improved thermal performance can lead to substantial energy savings in practical systems by reducing the required heat exchange area or pumping power for the same thermal duty. This enhancement is particularly beneficial in industrial applications such as compact heat exchangers, solar thermal collectors, automobile radiators, and process cooling systems.

The future work can be extended with combinations of perforations on the twisted tape inserts and using ternary nanofluids. The ternary nanofluids have higher thermal conductivity when compared to base fluid and HNFs. By introducing the perorations on TT inserts may reduce the pressure drop. Additionally, optimization study can also be performed to obtain the best possible combination of twisted tape insert parameters in terms of maximum possible heat transfer rate with least amount of pressure drop.

Author contribution statement

Pidaparthy Maheshbabu: Conceptualization, Methodology, Validation, Investigation, software, Writing – original draft. Ramkumar Ramkrishnan: Formal analysis, Review & editing, Goda Sreenivasulu Reddy: Investigation, Formal analysis, Review & editing, Prakash H. Jadhav: Conceptualization, Methodology, Investigation, formal analysis, Writing original draft, Review & editing.

Declaration of interests

The authors declare there is no conflict of interest between the contents of this work and any reported studies.

Data availability

The data supporting the findings of this study are available from the authors upon reasonable request.

Declaration of generative AI and AI-assisted technologies in the writing process

No generative AI or AI-assisted technologies were used in the writing, analysis, or preparation of this manuscript.

Nomenclature

L	Length of pipe (m)
d	Pipe ID (m)
FF	Friction factor
TR	Twist ratio
LT	Twist length (mm)
PT	Plain tube
Q_{avg}	Average heat transfer rate (W)
TKE	Turbulent kinetic energy
HNFs	Hybrid nanofluids
ΔT_{LMTD}	Log mean temperature difference
CFHEx	Counter flow heat exchanger
D	Pipe OD (m)
A	Pipe area (m^2)
T	Temperature (°C)
ΔP	Pressure drops (Pa)
w	Width (mm)
HEx	Heat exchanger
Q	Heat transfer rate (W)
PEC	Performance evaluation criteria
TT	Twisted tape
ΔT	Temperature difference (°C)
BFW	Base fluid water

Greek Symbols

C_p	Specific heat (J/kg-°C)
ρ	Fluid Density (kg/m^3)
μ	Dynamic viscosity (N-s/m)

υ	Kinematic viscosity (m^2/s)
φ	Volume of hybrid nanofluids concentrations
U_i	Overall heat transfer coefficient (W/m^2K)
K	Thermal conductivity (W/mK)
Pr	Prandtl number
Nu	Nusselt number
Re	Reynolds number
$\dot{m}$	Mass flow rate (kg/s)
h	Heat transfer coefficient (W/m^2K)

Subscripts

c	Cold fluid
i	inlet
n_f	nanofluids
Hyb.	Hybrid
h	Hot fluid
o	outlet
b_f	Base fluid

References

[1] Maddah H, Alizadeh M, Ghasemi N, Wan Alwi SR. Experimental study of Al_2O_3/water nanofluid turbulent heat transfer enhancement in the horizontal double pipes fitted with modified twisted tapes. Int J Heat and Mass Transf 2014;78: 1042–1054. https://doi.org/10.1016/j.ijheatmasstransfer.2014.07.059.

[2] Suneetha S, Subbarayudu K, Anki Reddy PB. Hybrid nanofluids developents and benefits: A comprehensive review. J Therm Engi 2022; 8:445-455. https://doi.org/10.18186/thermal.1117455.

[3] Pulgam MKR, Rout SK, Sarangi SK. Astste-of-the-art review on thermo fluid performance of brazed plate heat exchanger for HVAC application. J Therm Engi 2024; 10:1390-1410. https://doi.org/10.14744/thermal.0000869.

[4] Aruna J, Niranjan H. Effects of electric field, MHD micropolar hybrid nanofluid flow with mixed convection and thermal rediation across a flat surface. J Therm Engi 2024; 10:1607-1620. https://doi.org/10.14744/thermal.0000851.

[5] Nazari M, Ashouri M, Kayhani MH, Tamayol A. Experimental study of convective heat transfer of a nanofluid through a pipe filled with metal foam. Int J Therm Sci 2015;88: 33–39. https://doi.org/10.1016/j.ijthermalsci.2014.08.013.

[6] Jadhav PH, Gnanasekaran N. Optimum design of heat exchanging device for efficient heat absorption using high porosity metal foams. Int Comm Heat and Mass Transf 2023;126: 105475. https://doi.org/10.1016/j.icheatmasstransfer.2021.105475.

[7] Jadhav PH, Gnanasekaran N, Mobedi M. Analysis of functionally graded metal foams for the accomplishment of heat transfer enhancement under partially filled condition in a heat exchanger. Ener 2022;263: 125691. https://doi.org/10.1016/j.energy.2022.125691.

[8] Jadhav PH, Gnanasekaran N, Perumal DA, Mobedi M. Performance evaluation of partially filled high porosity metal foam configurations in a pipe. Appl Therm Engi 2021;194: 117081. https://doi.org/10.1016/j.applthermaleng.2021.117081.

[9] Jadhav PH, Trilok G, Gnanasekaran N, Mobedi M. Performance score based multi-objective optimization for thermal design of partially filled high porosity metal foam pipes under forced convection. Int J Heat and Mass Transf 2021; 182:121911. https://doi.org/10.1016/j.ijheatmasstransfer.2021.121911.

[10] Jadhav PH, Gnanasekaran N, Perumal DA. Numerical Consideration of LTNE and Darcy Extended Forchheimer Models for the Analysis of Forced Convection in a Horizontal Pipe in the Presence of Metal Foam. J Heat Transf 2021;143: 1–16. https://doi.org/10.1115/1.4048622.

[11] Jadhav PH, Gnanasekaran N, Perumal DA. Conjugate heat transfer study comprising the effect of thermal conductivity and irreversibility in a pipe filled with metallic foams. Heat and Mass Transf 2021;57: 911-930. https://doi.org/10.1007/s00231-020-03000-x.

[12] Kamel MS, Al-Oran O, Lezsovits F. Thermal conductivity of Al_2O_3 and CeO_2 nanoparticles and their hybrid based water nanofluids: An experimental study. Periodica Poly Che Engi 2020;65: 50–60. https://doi.org/10.3311/PPch.15382.

[13] Hashim MW, Al-Zubaidi FN, Al-Salihi HA. Perfoamnce improvement of a decayed flow heat exchanger using spiral flow and nanofluid. J Therm Engi 2025; 11:508-518. https://doi.org/10.14744/thermal.0000930.

[14] Swetha D, Chalapathi KS, Saritha P. Performance Analysis of Shell and Tube Heat Exchanger using Nano Fluid. Int J Engg Res 2016;5: 320–325. https://doi.10.17577/IJERTV5IS100251.

[15] Bhuiya MMK, Sayem ASM, Islam M, Chowdhury MSU, Shahabuddin M. Performance assessment in a heat exchanger tube fitted with double counter twisted tape inserts ☆. Int Comm Heat and Mass Transf 2014;50: 25–33. https://doi.org/10.1016/j.icheatmasstransfer.2013.11.005.

[16] Shehram M, Hamidi MN, Wahab AAA, Desa MKM. Enhancing flat plate collectors' efficiency by minimizing optical losses through vacuum glazing and ethylene glycol-diamond-alumina nanofluid. J Therm Engi 2025; 11:550-576. https://doi.org/10.14744/thermal.0000932.

[17] Khoshvaght-Aliabadi M. Influence of different design parameters and Al_2O_3-water nanofluid flow on heat transfer and flow characteristics of sinusoidal-corrugated channels. Ener Conv and Mangmt 2014;88: 96–105. https://doi.org/10.1016/j.enconman.2014.08.042.

[18] Hemmat Esfe M, Hajmohammad H, Toghraie D, Rostamian H, Mahian O, Wongwises S. Multi-objective optimization of nanofluid flow in double tube heat exchangers for applications in energy systems. Ener 2017;137: 160–171. DOI: https://doi.org/10.1016/j.energy.2017.06.104.

[19] Krishna Varma KPV, Venkateswarlu K, Kalyani T, Hemalatha P, Vijaya Kumar P. Numerical analysis of spiral tube heat exchanger circulated with zinc oxide nanofluids. J Ther Eng 2025; 11:377-389. DOI: 10.14744/thermal.0000921.

[20] Azeez K, Abu Rahim AR, Ibraheem Ahmed R. Heat transfer enhancement for corrugated facing step channels using aluminum nitride nanofluid - numerical investigation. J Ther Eng 2022; 8:734-747. DOI: 10.18186/thermal.1197106.

[21] Paul A, Mani Nath J, Kanti Das T. An investigation of the MHD Cu-Al_2O_3/H_2O hybrid-nanofluid in a porous medium across a vertically stretching cylinder incorporating thermal stratification impact. J Ther Eng 2023; 9:799-810. DOI: 10.18186/thermal.1300847.

[22] Khargotra R, Kumar R, Nadda R, Dhingra S, Alam T. A review of different twisted tape configurations used in heat exchanger and their impact on thermal performance of the system. Heliy 2023;9: e16390. https://doi.org/10.1016/j.heliyon.2023.e16390.

[23] Li W, Yu Z, Wang Y, Li Y. Heat transfer enhancement of twisted tape inserts in supercritical carbon dioxide flow conditions based on CFD and vortex kinematics. Therm Sci Eng Prog 2022;31: 101285. https://doi.org/10.1016/j.tsep.2022.101285.

[24] Prasad PVD, Gupta AVSSKS, Deepak K. Investigation of Trapezoidal-Cut Twisted Tape Insert in a Double Pipe U-Tube Heat Exchanger using Al_2O_3/Water Nanofluid. Pro Mat Sci 2015;10: 50–63. https://doi.org/10.1016/j.mspro.2015.06.025.

[25] Varma KPVK, Venkateswarlu K, Kalyani T, Hemalatha S, Kumar PV. Numerical analysis of spiral tube heat exchanger circulated with zinc oxide nanofluids. J Therm Engi 2025; 11:377-389. https://doi.org/10.14744/thermal.0000921.

[26] Joseph PM, Arjunan STV, Sadanandam MMMN. Experimental and theoretical investigation on the effects of lower concentration CeO_2/water nanofluid in flat-plate solar collectors. J Therm Anal Calori 2019;135: 29-44. https://doi.org/10.1007/s10973-017-6865-4.

[27] Aghayari R, Maddah H, ourkiaei SM, Ahmadi MH, Chen L, Ghazvini M. Theoretical and experimental studies of heat transfer in a double-pipe heat exchanger equipped with twisted tape and nanofluid. The European Phy J Plus 2020; 123:252. https://doi.org/10.1140/epjp/s13360-020-00252-8.

[28] Kumar NTR, Bhramara P, Kirubeil A, Sundar LS, Singh MK, Sousa ACM. Effect of twisted tape inserts on heat transfer friction factor of Fe_3O_4 nano fluids flow in a double pipe U-bend heat exchanger. Int Comm Heat and Mass Transf 2018; 95:53–62. https://doi.org/10.1016/j.icheatmasstransfer.2018.03.020.

[29] Mirzaei M, Azimi A. Heat Transfer and Pressure Drop Characteristics of Graphene Oxide/Water Nanofluid in a Circular Tube Fitted with Wire Coil Insert. Expt Heat Transf 2016; 29:173-187. https://doi.org/10.1080/08916152.2014.973975.

[30] Pandey H, Gupta NK, Agrawal S. An experimental investigation to study the performance characteristics of heat pipe using aqueous hybrid nanofluids. J Ther Eng 2023;9: 1192-1201. DOI: 10.18186/thermal.1372260.

[31] Aruna J, Niranjan H. Effects of electric field, MHD micropolar hybrid nanofluid flow with mixed convection and thermal radiation across a flat surface. J Ther Eng 2024;10: 1607-1620. 31:85-105. DOI: 10.14744/thermal.0000851.

[32] Narendran G, Jadhav PH, Gnanasekaran N. Numerical analysis of thermo hydro-dynamics behavior of solar flat plate collector with square and V-cut twisted tape inserts. Num Heat Transf Part A: Appl 2023; 86:2664-2688. https://doi.org/10.1080/10407782.2023.2294043.

[33] Narendran G, Jadhav PH, Gnanasekaran N. A smart and sustainable energy approach by performing multi-objective optimization in a minichannel heat sink for waste heat recovery applications. Sust Ener Techn Assess 2023; 60:103447. https://doi.org/10.1016/j.seta.2023.103447.

[34] Reddy GS, Kalaivanan R, Kumar RU, Jadhav PH. Influence of W-cut twisted tape inserts on heat transfer characteristics of a counter flow heat exchanger using CeO_2 nanofluid – an experimental and numerical investigations. Num Heat Transf Part A: Appl 2024; 0:1–21. https://doi.org/10.1080/10407782.2024.2359060.

[35] Goda SR, Kalaivanan R, Kumar RU, Jadhav PH. Experimental and numerical investigation of thermo-hydrodynamic performance of twin tube counter flow heat exchanger using cerium oxide nanofluid, Num Heat Transf Part A: Appl 2023;86: 613-631. https://doi.org/10.1080/10407782.2023.2268831.

[36] Kumar B, Kumar M, Patil AK, Jain S. Effect of V cut in perforated twisted tape insert on heat transfer and fluid flow behavior of tube flow: An experimental study. Expt Heat Transf 2018; 32:524-544. https://doi.org/10.1080/08916152.2018.1545808.

[37] Murthy SMH, Hegde RN. Investigations on the effect of disturbed flow using differently configured turbulators and Alumina nanofluid as a coolant in a double tube heat exchanger. Expt Heat Transf 2021;35: 282-307. https://doi.org/10.1080/08916152.2020.1860159.

[38] Kumar A, Sharma S, Kumar S, Maithani R. Thermohydraulic analysis of twisted tape inserts with SiO_2 / H_2O nanofluid in heat exchanger," Australian J Mech Eng 2021; 21: 1184-1197. https://doi.org/10.1080/14484846.2021.1960672.

[39] Bhattad A. Experimental investigation of Al_2O_3 – MgO hot hybrid nanofluid in a plate heat exchanger. Heat Transf 2020;49: 2344-2354. https://doi.org/10.1002/htj.21724.

[40] Mund A, Pattanayak B, Jayakumar JS, Parashar K, Parashar SKS. Experimental and Numerical Study of Heat Transfer in Double-Pipe Heat Water Nano fluid. Adv in Fluid and Therm Eng 2019; 531-540. https://doi.org/10.1007/978-981-13-6416-7.

[41] Ahmed W, Chowdhury SNKZZ, Naveed MRBJ, Mujtaba AMA. Experimental investigation of convective heat transfer growth on ZnO@TiO_2/DW binary composites/hybrid nanofluids in a circular heat exchanger. J Therm Anal Calori 2021;143: 879-898. https://doi.org/10.1007/s10973-020-09363-x.

[42] Plant RD, Hodgson GK, Impellizzeri S, Saghir MZ. Experimental and numerical investigation of heat enhancement using a hybrid nanofluid of copper oxide/alumina nanoparticles in water. J Therm Anal Calori 2020; 141:1951–196. https://doi.org/10.1007/s10973-020-09639-2.

[43] Singh SK, Sarkar J. Experimental hydrothermal characteristics of concentric tube heat exchanger with V-cut twisted tape turbulator using PCM dispersed mono/hybrid nanofluids. Expt Heat Transf 2021;34: 421-442. https://doi.org/10.1080/08916152.2020.1772412.

[44] Hamza NFA, Aljabair S. Heliyon Evaluation of thermal performance factors by hybrid nanofluid and twisted tape inserts in heat exchanger. Heliy 2022;8: e11950. https://doi.org/10.1016/j.heliyon.2022.e11950.

[45] Maheshbabu P, Ramkumar R, Reddy GS, Bakkiyaraj, M, Jadhav PH. Numerical investigation of MWCNT/ZnO hybrid nanofluid heat performance of a counter flow heat exchanger. J Mech Conti and Mathem Sci 2025; 20:136-153. https://doi.org/10.26782/jmcma.2025.07.00008.

[46] Alhajaj Z, Bayomy AM, Saghir MZ, Rahman MM. Flow of nanofluid and hybrid fluid in porous channels: Experimental and numerical approach. Int J Thermo 2020;1-2: 100016. https://doi.org/10.1016/j.ijft.2020.100016.

[47] Jadhav PH, Sandhya V, Reddy VJ, Reddy GS, Gnanasekaran N, Harsur S. Thermal performance evaluation and entropy generation analysis of partially filled aluminum metal foam heat exchanger. Int J Heat and Fluid Flow 2026; 117:110109. https://doi.org/10.1016/j.ijheatfluidflow.2025.110109.

[48] Jadhav PH, Gnanasekaran N, Perumal DA. Thermodynamic analysis of entropy generation in a horizontal pipe filled with high porosity metal foams. Materials Today: Procedings 2022; 51:1598-1603. https://doi.org/10.1016/j.matpr.2021.10.451.

[49] Jadhav PH, Kotresha B, Gnanasekaran N, Perumal DA. Forced Convection Analysis in a Horizontal Pipe in the Presence of Aluminium Metal Foam—ANumerical Study. Fluid Mechanics and Fluid Power, Lecture Notes in Mechanical Engineering 2021:491-498. https://doi.org/10.1007/978-981-16-0698-4_53.

[50] Athith TS, Trilok G, Jadhav PH, Gnanasekaran N. Heat transfer optimization using genetic algorithm and artificial neural network in a heat exchanger with partially filled different high porosity metal foam. Materials Today: Proceedings 2022; 51:1642-1648. https://doi.org/10.1016/j.matpr.2021.11.248.

[51] Rout SK, Thatoi DN, Acharya AK, Mishra DP. CFD supported performance estimation of an internally finned tube heat exchanger under mixed convection flow. Proc Eng 2012; 38:585-597. doi: https://doi.org/10.1016/j.proeng.2012.06.073.

[52] Pulagam MKR, Rout SK, Muduli KK, Syed SA, Barik D, Hussein AK. Internal Finned Heat Exchangers: Thermal and Hydraulic Performance Review. Int J Heat and Tech 2024;42:583-592. https://doi.org/10.18280/ijht.420225.

[53] Rout SK, Hussein AK. MULTI - OBJECTIVE OPTIMIZATION of A THREE-DIMENSIONAL INTERNALLY FINNED TUBE BASED ON RESPONSE SURFACE METHODOLOGY (RSM). J Therm Eng 2015; 1:131-142. https://doi.org/10.18186/jte.82948.

[54] Rout SK, Mishra DP, Thatoi DN, Acharya AK. NumericalAnalysis of MixedConvectionthrough anInternally Finned Tube. Adv Mech Eng 2012;918342. https://doi:10.1155/2012/918342.

[55] Mahfoud B. Mahfoud HE. Magnetohydrodynamics Flow of Hybrid Nanofluid Rotating in Annulus Through Two Coaxial Cylinders. J Thermophysics Heat Transf 2025;39. https://doi.org/10.2514/1.T7035.

[56] Mahfoud B. Enhancement Heat Transfer of Swirling Nanofluid Using an Electrical Conducting Lid. J Thermophysics Heat Transf 2023; 37:263-271. DOI: 10.2514/1. T6550.

[57] Mabood F, Akinshilo AT. Stability analysis and heat transfer of hybrid Cu-Al transport over a stretching surface. Int Comm Heat Mass Transf 2021; 123:105215. https://doi.org/10.1016/j.icheatmasstransfer.2021.105215.

[58] Akinshilo AT, Mabood F, Ilegbusi AO. Heat generation and nonlinear radiation effects on MHD Casson nanofluids over a thin needle embedded in porous medium. Int Comm Heat Mass Transf 2021; 127:105547. https://doi.org/10.1016/j.icheatmasstransfer.2021.105547.

[59] Asokan N, Gunnasegaran P, Vicki V. Experimental investigation on the thermal performance of compact heat exchanger and the rheological properties of low concentration mono and hybrid nanofluids having Al_2O_3 and CuO nanoparticles. Therm Sci Eng Prog 2020; 20:100727. https://doi.org/10.1016/j.tsep.2020.100727.

[60] Ramadhan AI, Azmi WH, Mamat R, Hamid KA. Experimental and numerical study of heat transfer and friction factors of plain tube with hybrid nanofluids. Case Stud Therm Eng 2020; 22:100782. https://doi.org/10.1016/j.csite.2020.100782.

[61] Bhattad A, Sarkar J. Hydrothermal performance of plate heat exchanger with an alumina-graphene hybrid naofluid: experimental study. J Brazi Soc Mech Sci Eng 2020; 42:377. https://doi.org/10.1007/s40430-020-02459-3.

[62] Somasundaram U, Pichumani M. How does the tunable magnetic response and synergy in spinel-type manganese ferrite-graphene oxide hybrid nanofluids govern the thermal efficiency and flow dynamics in shell and helically coiled tube heat exchangers? J Brazi Soc Mech Sci Eng 2025; 47:218. https://doi.org/10.1007/s40430-025-05528-7.

[63] Maheshbabu P, Ramkrishnan R. Influence of MWCNT/ZnO hybrid characteristics for heat transfer applications. J Nano Nanoengg and Nanosy 2024;1 - 12. DOI: 10.1177/23977914241289251.

[64] Ansys Southpointe, ANSYS Fluent Theory Guide, ANSYS Inc., USA. 15317 (2013) 724–746.

[65] Elias MM, Shahrul IM, Mahbubul IM, Saidur R, Rahim NA. Effect of different nanoparticle shapes on shell and tube heat exchanger using different baffle angles and operated with nanofluid. Int J Heat and Mass Transf 2014; 70:289–297. https://doi.org/10.1016/j.ijheatmass transfer.2013.11.018.

[66] Kannaiyan S, Boobalan C, Umasankaran A, Ravirajan A, Sathyan S, Thomas T. Comparison of experimental and calculated thermophysical properties of alumina/cupric oxide hybrid nanofluids. J Mol Liqu 2017; 244:469-477. https://doi.org/10.1016/j.molliq.2017.09.035.

[67] Takabi B, Salehi S. Augmentation of the Heat Transfer Performance of a Sinusoidal Corrugated Enclosure by Employing Hybrid Nanofluid. Adv Mech Eng 2014; 1 - 16. https://dx.doi.org/10.1155/2014/147059.

[68] Zhang X, Li J, Zhang Y. Heat transfer characteristics of nanofluid under the action of magnetic field based on molecular dynamics and flow states. Num Heat Transf Part A: Appl 2024;85:491-515. https://doi.org/10.1080/10407782.2023.2187904.

[69] Petukhov BS. Heat transfer and friction in turbulent pipe flow with variable physical properties. Adv Heat tranaf 1970;6: 503-564. https://doi.org/10.1016/S0065-2717(08)70153-9.

[70] Irshad K, Islam N, Zahir MH, Pasha AA, Abdelgawad AF. Thermal performance investigation of Therminol55/MWCNT+CuO nanofluid flow in a heat exchanger from an exergy and entropy approach. Case Stud Therm Eng 2022;34: 102010. https://doi.org/10.1016/j.csite.2022.102010.

[71] Jadhav PH, Reddy GS, Priyadarsini Ch. I, Reddy VJ, Bireddy RS, Gnanasekaran N. Performance evaluation of partially filled metal foam sinusoidal corrugated channel heat exchanger for waste heat recovery system. Thermal Advances 2026; 6:100100. https://doi.org/10.1016/j.thradv.2026.100100.